**Distribution Agreement**

In presenting this thesis as a partial fulfillment of the requirements for a degree from Emory University, I hereby grant to Emory University and its agents the non-exclusive license to archive, make accessible, and display my thesis in whole or in part in all forms of media, now or hereafter now, including display on the World Wide Web. I understand that I may select some access restrictions as part of the online submission of this thesis. I retain all ownership rights to the copyright of the thesis. I also retain the right to use in future works (such as articles or books) all or part of this thesis.

Kristina Trifonova April 10, 2023

# Optimizing a Bifurcating [NiFe]-Hydrogenase System for Light-Driven Hydrogen Production

by

Kristina Trifonova

R. Brian Dyer
Adviser

Chemistry

R. Brian Dyer

Adviser

Frank McDonald

Committee Member

Katherine Davis

Committee Member

2023

# Optimizing a Bifurcating [NiFe]-Hydrogenase System for Light-Driven Hydrogen Production

By

Kristina Trifonova

R. Brian Dyer

Adviser

An abstract of
a thesis submitted to the Faculty of Emory College of Arts and Sciences
of Emory University in partial fulfillment
of the requirements of the degree of
Bachelor of Science with Honors

Chemistry

2023

Abstract

Optimizing a Bifurcating [NiFe]-Hydrogenase System for Light-Driven Hydrogen Production
By Kristina Trifonova

Electron confurcation is a recently discovered biological mechanism that enables an unfavorable electron transfer by coupling it with a favorable electron transfer to produce high-energy intermediates without using ATP. [NiFe]-hydrogenase in the anaerobic bacteria *Acetomicrobium mobile* uses electron confurcation to reversibly convert protons and electrons to hydrogen gas. We probe its mechanism and develop an artificial photosynthetic system for light-driven hydrogen production by coupling *A. mobile* hydrogenase with photosensitive semiconductor nanomaterials. CdSe quantum dots with the desired optical and electronic properties were engineered, and we demonstrate their ability to initiate electron confurcation in hydrogenase when illuminated. We tested numerous reaction conditions to optimize $H_2$ production and found evidence that the CdSe quantum dots bind to hydrogenase and inhibit its ability to perform electron confurcation. This adds support to the theory that conformational changes are key to electron confurcation in *A. mobile* hydrogenase.

# Optimizing a Bifurcating [NiFe]-Hydrogenase System for Light-Driven Hydrogen Production

By

Kristina Trifonova

R. Brian Dyer

Adviser

A thesis submitted to the Faculty of Emory College of Arts and Sciences
of Emory University in partial fulfillment
of the requirements of the degree of
Bachelor of Science with Honors

Chemistry

2023

Acknowledgements

Reaching the end of an undergraduate degree, especially one with honors, is impossible without overcoming much uncertainty and many roadblocks. I feel very privileged to have had the support and guidance of so many fellow students and faculty members at Emory during this time of growth and learning.

First, I want to express my gratitude to Dr. Dyer for his guidance. Thank you for welcoming me into your lab, always pushing me to become a better scientist, and investing in my future. My time in the Dyer Lab has been so formative, and I will always look back fondly on the community I found there.

Next, I would like to thank Seth Wiley, my mentor. I am grateful for your unbelievable patience as I learned the ropes in lab and for your sense of humor. Thank you for all your help with my applications, project meetings, and experimental planning and, most importantly, for always reminding me that research and school are not all that there is in life – I will certainly carry this lesson with me as I begin my PhD next fall.

I am also incredibly grateful to have lab mates who always make me laugh – thank you to Sam Lee, Sarah Bell, and Ritika Pandey. Alexia Prokopik, David White, and Caterina Netto have also been amazing role models, and I am so grateful to you for adopting me as your unofficial mentee in the last spring of my senior year.

I would also like to extend thanks to my committee members. I know that this is a very busy period in the semester, and I greatly appreciate the time and energy you have dedicated to my thesis defense.

Table of Contents

**Chapter 1: An Introduction to Hydrogenase and Electron Bifurcation** 1

1.1 The Energy Crisis 1

1.1.1 Motivation: The Need for Renewable Energy and Challenges 1

1.1.2 Energy Conversion in Nature 3

1.2 Overview of Hydrogenase Metalloenzymes 3

1.2.1 Properties of [NiFe]-Hydrogenases 3

1.2.2 *Acetomicrobium mobile* Hydrogenase: Properties 4

1.3 Electron Bifurcation 5

1.3.1 An Overview of Electron Bifurcation 5

1.3.2 *Acetomicrobium mobile* Hydrogenase: Mechanism 6

1.4 Proposed Model System 8

1.5 Scope and Aims 8

1.6 References 9

**Chapter 2: Developing Photosensitive Semiconductor Nanomaterials** 11

2.1 Introduction 11

2.2 Methodology 13

2.2.1 CdSe Quantum Dot Synthesis 13

2.2.2 CdSe/CdS Dot-in-Rod Synthesis 13

2.2.3 Ligand Exchange 14

2.2.4 Nanomaterial Characterization and Quantum Efficiency Evaluation 14

2.2.5 Steady-State Photoreduction of Ferredoxin 15

2.3 Results and Discussion 16

2.3.1 Characterization of Nanomaterials 16

2.3.2 Steady-State Photoreduction of Ferredoxin 18

2.4 References 20

**Chapter 3: Optimizing System Parameters for Light-Driven Hydrogen Production** 22

3.1 Introduction 22

3.2 Methodology 23

3.2.1 Hydrogenase Activity Assay 23
3.2.2 Preparation of Sample for Hydrogen Production Assay 24
3.2.3 Effect of FMN Concentration on Electron Bifurcation Rate 24
3.2.4 Photoluminescence Quenching of CdSe Quantum Dots 25
3.3 Results and Discussion 25
3.3.1 Hydrogenase Activity Assays 25
3.3.2 Hydrogen Production Assays 26
3.3.3 Effect of FMN Concentration on Electron Bifurcation Rate 30
3.3.4 Photoluminescence Quenching of CdSe Quantum Dots 31
3.4 References 32
**Chapter 4: Conclusions and Perspectives** 33
4.1 Aim 1: Engineering Effective Photosensitive Nanomaterials 33
4.2 Aim 2: Achieving Light-Driven Reduction of *Amo* Ferredoxin 33
4.3 Aim 3: Identifying Conditions for $H_2$ Production via Electron Confurcation 34
4.4 Implications and Future Directions 34

**List of Figures**

**Figure 1.1** Growth of energy demand in the US 1

**Figure 1.2** The “duck curve” 2

**Figure 1.3** Hydrogenase active site structures 4

**Figure 1.4** Hydrogenase subunits 5

**Figure 1.5** Electron bifurcation vs. confurcation in hydrogenase 6

**Figure 1.6** Pathway of electron transfer through HydABCSL 7

**Figure 1.7** HydABCSL conformational changes 7

**Figure 1.8** Diagram of proposed model system 8

**Figure 2.1** UV-Vis changes with FMN and Fd reduction 12

**Figure 2.2** Quantum yield experiment set up 15

**Figure 2.3** Nanomaterial characterization 16

**Figure 2.4** Light-induced potential jump of dot-in-rods 17

**Figure 2.5** Steady-state photoreduction of *Pfu* ferredoxin 18

**Figure 2.6** Steady-state photoreduction of *Amo* ferredoxin 19

**Figure 3.1** Expected rate of pressure production via electron bifurcation 23

**Figure 3.2** Hydrogenase activity assay results 26

**Figure 3.3** Hydrogen production assay: *Tma* hydrogenase 27

**Figure 3.4** Hydrogen production assay: *Amo* hydrogenase 28

**Figure 3.5** Rate of ferredoxin reduction depends on hydrogenase concentration 29

**Figure 3.6** Hydrogen production assay: 600 nM *Amo* hydrogenase 29

**Figure 3.7** Hydrogen production assay: *Amo* Fd 30

**Figure 3.8** Rate of electron bifurcation before and after FMN addition 31

**Figure 3.9** Photoluminescence quenching assay of quantum dots 32

# Chapter 1: An Introduction to Hydrogenase and Electron Bifurcation

## 1.1 The Energy Crisis

### *1.1.1 Motivation: The Need for Renewable Energy and Challenges*

The need for renewable energy has never been more urgent than it is today. Exponential population growth and global industrialization result in annually increasing demands for energy **(Figure 1.1)** [1]. Each year, a larger fraction of the global energy supply comes from nonrenewable energy sources, even though society is now aware of the long-lasting and hazardous environmental repercussions that accompany their use [2]. Burning coal, natural gases, and oil emits greenhouse gases like $CO_2$ and methane that trap heat in the Earth's atmosphere and cause worsening climate threats, including sea-level rise and more severe natural disasters, in addition to documented health and economic risks [3].

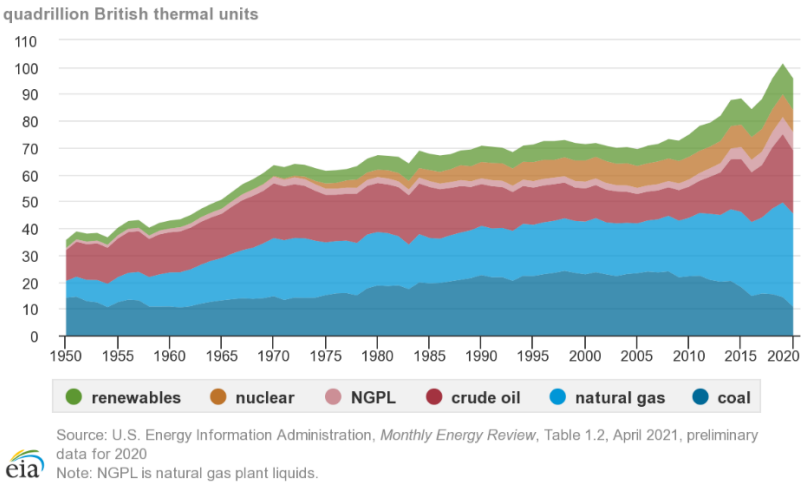


**Figure 1.1** Growth of energy production by source between 1950-2020 in the United States [3].

As the need to phase out fossil fuels has gained the attention of governments and consumers, renewable energy sources have become more prominent in society. In particular, solar energy – obtained by converting sunlight into electricity and heat – has been widely embraced. The use of solar cells which convert sunlight to electricity is growing, and the International Energy Agency reports that the energy use from solar photovoltaics grew by 22% in 2021, accounted for 3.6% of all energy generated across the globe, and was the third largest renewable energy source behind wind and hydropower [4]. However, large-scale integration of solar energy with existing energy infrastructure does not come without challenges.

The biggest obstacle to wide-scale implementation of solar cells, is the misalignment of peak demand and supply times. Photovoltaics produce the most electricity at mid-day when the sun is out, while the highest energy demands are in the evenings when people are returning home from work, turning on lights, and using appliances. Additionally, solar energy is an intermittent energy source rather than a dispatchable one, because its energy production is determined by cloud cover, location, and time of day and cannot be easily switched on and off [5]. Thus, photovoltaics must be integrated with traditional energy sources to fully meet demand. To avoid energy overproduction, dispatchers must ramp the amount of energy produced by power plants up or down, depending on how much electricity is being produced by photovoltaics [5].

In 2013, the California Independent System Operator published the "duck curve" (**Figure 1.2)**, which projects how increases in solar energy use will steepen the energy ramp up that generators must perform to meet evening energy demands, as solar energy contribution wanes [6]. They project a required ramp up of approximately 13,000 MW in three hours by 2020, an unsustainable rate which could result in voltage violations and high energy losses [7]. Potential solutions to the overproduction problem include developing more accurate forecasts of energy needs or storage methods for solar energy generated at non-peak demand times.

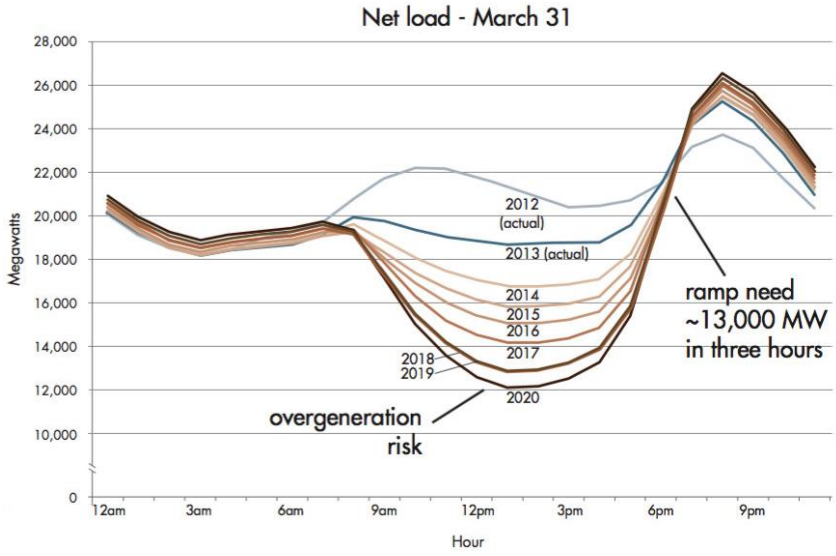


**Figure 1.2**. The "duck curve" projects how an increase in solar panels in California from 2012-2020 will increase the grid ramp up needed to meet demands between 3PM and 6PM, creating an overproduction risk [6].

### *1.1.2 Energy Conversion in Nature*

Nature has already developed a mechanism for harvesting and storing energy from sunlight using photosynthesis. In this process, sunlight excites electrons in the plant's chloroplasts that cause water to split into oxygen, protons, and electrons. The electrons are ultimately used to form glucose, which the plant stores and later breaks down for energy. Artificial photosynthesis, which stores energy from light in the bonds of chemical fuels like $H_2$ and ammonia, is one potential route for solar energy storage [8]. Hydrogen solar fuels could be easily used in hydrogen-based fuel cells, which generate energy from hydrogen and oxygen with up to 60% efficiency and water as the only byproduct [9].

Nature has also developed metalloenzymes, which are a class of protein catalysts that contain a metal in their active site, for driving such redox reactions. Metalloenzymes are known to facilitate various oxidation and reduction reactions that are critical to metabolic energy conversion processes. Research efforts over the last decade have showed that when coupled with light-harvesting molecules, metalloenzymes can drive photocatalytic systems that convert light into various chemical products. Although most have low conversion efficiencies, artificial photosynthetic systems involving metalloenzymes have provided useful insights and design principles for bio-inspired engineering of energy conversion mechanisms [10].

## 1.2 Overview of Hydrogenase Metalloenzymes

### *1.2.1 Properties of [NiFe]-Hydrogenases*

Hydrogenases are metalloenzymes that facilitate the reversible reduction of protons to hydrogen gas. Due to their oxygen sensitivity, they are mostly found in anaerobic microorganisms, which use hydrogenase in their metabolisms to either generate electrons or easily eliminate excess reductant, even if no electron acceptors except protons are available. There are three types of evolutionarily unrelated hydrogenases that differ in their active site metals: [NiFe]-hydrogenases, [FeFe]-hydrogenases, and [Fe]-hydrogenases, depicted in **Figure 1.3**. Typically, [NiFe]-hydrogenases are less active than [FeFe]-hydrogenases and are more primed for hydrogen oxidation than hydrogen production [11]. A shared characteristic between [NiFe]- and [FeFe]-hydrogenases is a series of [Fe-S] clusters that act as an electron-conducting wire, allowing electrons to flow from the protein's surface to its active site [12].

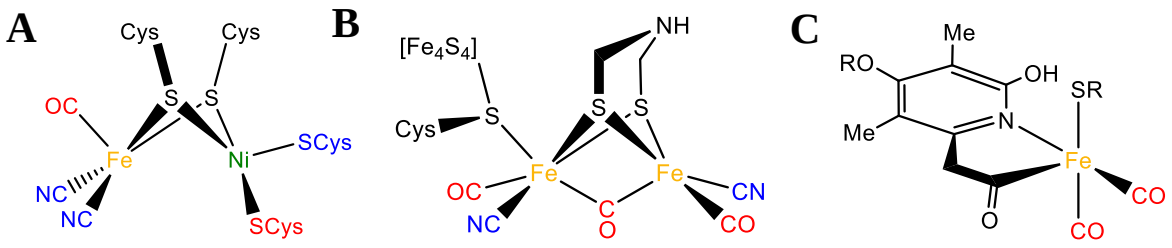


**Figure 1.3 (A)** [NiFe]-hydrogenase active site. **(B)** [FeFe]-hydrogenase active site and H-cluster. **(C)** [Fe]-hydrogenase active site. [12]

Systems coupling photosensitive semiconductor nanomaterials with hydrogenases for artificial photosynthesis have been successfully optimized with varying turnover frequencies and conversion rates. For instance, a turnover frequency of 50 $s^{-1}$enzyme$^{-1}$ was reported for a system of [NiFeS]-hydrogenase from *Desulfomicrobium baculatum* coupled with $TiO_2$ nanoparticles, even when using natural light from the sky to excite the system [13]. More recently, a system using CdS nanorods with *Clostridium acetobutylicum* [FeFe] hydrogenase I showed an impressive turnover frequency of 380-900 $s^{-1}$enzyme$^{-1}$ with a photon conversion rate of up to 20% [14]. Although there is precedent for coupling semiconductors with hydrogenase for light-driven hydrogen production, much remains to be learned about the mechanisms of these systems, as each one is unique.

*1.2.2 Acetomicrobium mobile Hydrogenase: Properties*

*Acetomicrobium mobile* is an anaerobic, thermophilic bacterium that grows in wastewater treatment facilities [15]. It was recently discovered that *A. mobile* bacteria contains a structurally unique [NiFe]-hydrogenase [16]. Most [NiFe]-hydrogenases contain two subunits: a small and large one (**Figure 1.4A**). In contrast, typical [FeFe]-hydrogenases contain three subunits: A, B, and C, with a so-called H-cluster in the A subunit which is the active site of the molecule (**Figure 1.4B**). *A. mobile* hydrogenase, on the other hand, contains five subunits: three which are homologs of the [FeFe]-hydrogenase A, B, and C subunits and two which are homologs of the [NiFe]-hydrogenase S and L subunits, making it an evolutionarily interesting protein **(Figure 1.4C)**. In addition, *A. mobile* hydrogenase (HydABCSL) makes use of a poorly understood energy conservation mechanism called electron bifurcation, which only a handful of other hydrogenase species use [16]. The distinctive structure and mechanism of *A. mobile* HydABCSL

make its chemistry interesting and useful to study, both to obtain fundamental knowledge about its mechanism and to gain new inspiration for engineering photosynthetic systems.

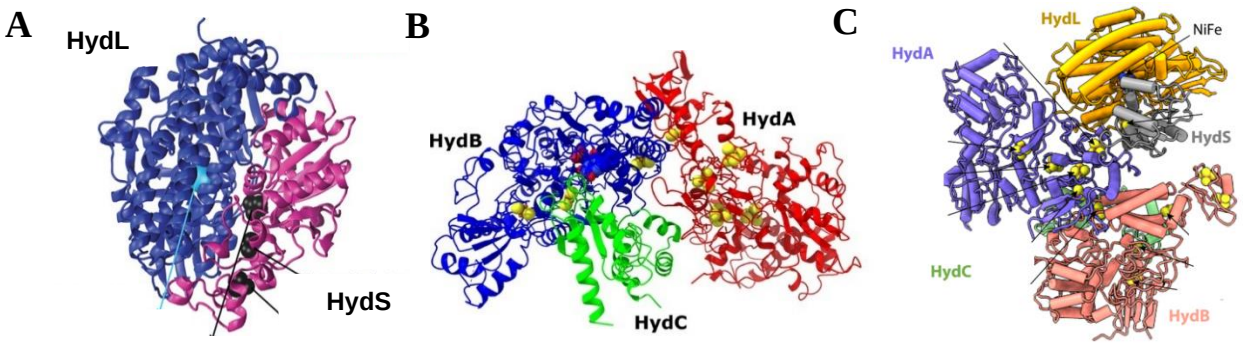


**Figure 1.4. (A)** L and S subunits in [NiFe]-hydrogenases [17] **(B)** A, B, and C subunits in [FeFe]-hydrogenases [18] **(C)** A, B, C, S, and L subunits in *A. mobile* [NiFe]-hydrogenase [16]

## 1.3 Electron Bifurcation

### *1.3.1 An Overview of Electron Bifurcation*

Electron bifurcation is a powerful thermodynamic process in which an otherwise unfavorable electron transfer is enabled by coupling it to a favorable electron transfer (**Figure 1.5**). In biology, long chains of exergonic electron transfers are wasteful, as free energy is lost to heat. Electron bifurcation is thus an incredible fundamental mechanism that makes biological systems more efficient and accomplishes the thermodynamically challenging task of producing high-energy electrons capable of performing work in the system without using ATP [19].

The general mechanism of electron bifurcation involves a two-electron donor and two electron acceptors – one with high potential and low energy and one with low potential and high energy. First, the donor transfers two electrons to an intermediate two-electron acceptor molecule that serves as the bifurcation site. Typically, the bifurcating cofactor has inverted reduction potentials, meaning that its first reduction potential is lower than the second [20]. Thus, the electrons are split, as the first undergoes a favorable transfer to a high potential acceptor and the other is unfavorably transferred to the low potential acceptor. In *Amo* hydrogenase, the natural cofactors involved in electron bifurcation are flavin mononucleotide (FMN) which is the bifurcating cofactor, oxidized ferredoxin (Fd) which is the low potential acceptor, and $NAD^+$ which is the high potential acceptor **(Figure 1.5A)** [16].

The reverse of electron bifurcation, called electron confurcation, is the mechanism that HydABCSL uses to generate hydrogen **(Figure 1.5B)**. In electron confurcation, one high-energy electron from reduced Fd and one low-energy electron from NADH are donated to the bifurcating cofactor FMN, which transfers the two electrons to an [Fe-S] cluster chain that eventually leads them to the active site where they reduce protons to hydrogen gas [16]. Since the focus of this thesis is on applications of metalloenzyme energy conversion schemes for solar fuel synthesis, electron confurcation was the primary reaction studied.

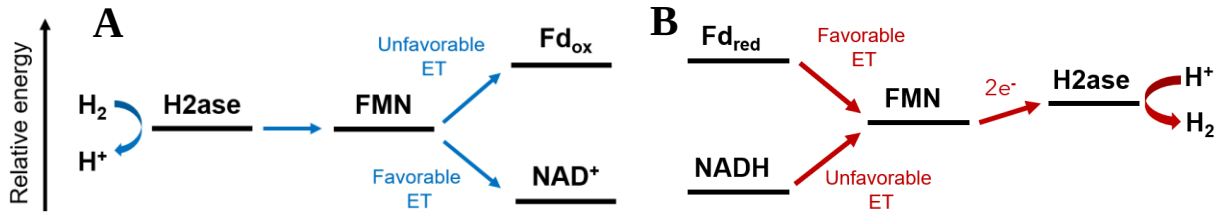


**Figure 1.5 (A)** Electron bifurcation scheme in HydABCSL. **(B)** Electron confurcation scheme in HydABCSL.

*1.3.2 Electron Bifurcation in Acetomicrobium mobile Hydrogenase*

Based on structure and distance between adjacent [Fe-S] clusters, cryo-electron microscopy data of HydABCSL has provided initial insights into the electron transfer pathway through the protein to from hydrogen to Fd and $NAD^+$. Electrons can tunnel between [Fe-S] clusters that are approximately 14Å or less apart, which is a useful threshold that was used to assess the likelihood of a particular electron transfer pathway [21]. As can be seen in **Figure 1.6**, the first proposed step of the mechanism involves $H_2$ reduction at the [NiFe] active site in HydL. After this, electrons are shuttled along the [Fe-S] cluster chain through the HydS and HydA subunits, until the electrons reach cluster B1 in the HydB subunit [16]. Electron transfer from the B1 cluster to FMN initializes the electron bifurcation process.

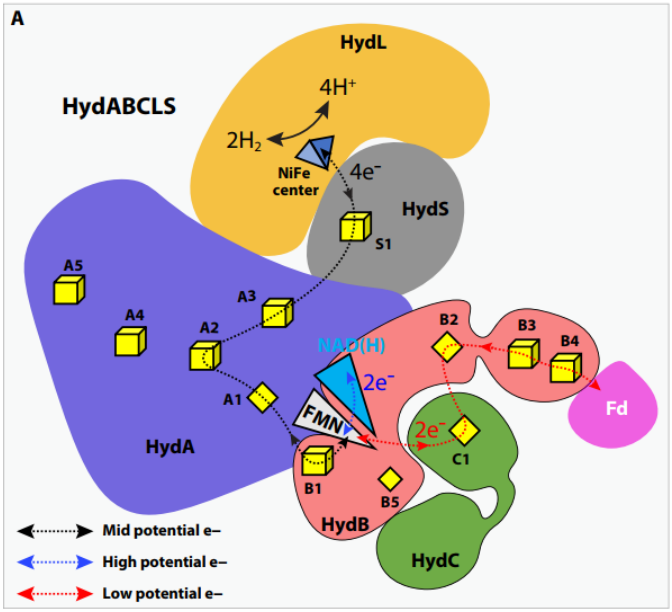


**Figure 1.6** Pathway of electron transfer through HydABCSL [16]

By characterizing the structure of HydABCSL in an unbound state and an FMN/NAD(H) bound state, it was suggested that the enzyme changes conformation to bring clusters B2, B3, and B4 closer to each other and moves the C1 cluster closer to FMN to facilitate electron transfer upon binding of FMN and NAD(H) **(Figure 1.7)**. Then, when Fd binds, another conformational change moves clusters C1 and B2 together, creating a path for Fd reduction and completing the bifurcation mechanism. Without these conformational changes, the [Fe-S] clusters are too far apart for electrons to traverse the full pathway for electron bifurcation [16]. Conformational changes thus seem elegantly gate electron flow from the low potential Fd back to FMN or $NAD^+$, which would short-circuit the system. Real-time kinetic data of the reaction would provide additional evidence to clarify the mechanism and provide new insights.

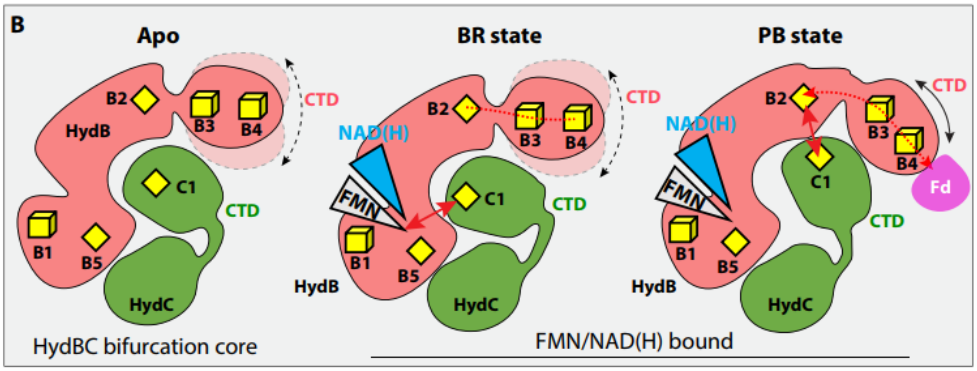


**Figure 1.7** Conformational changes of HydABCSL upon binding of cofactors [16].

## 1.4 Proposed Model System

To study light-driven electron confurcation in HydABCSL, a system coupling CdSe semiconductor nanoparticles with the enzyme is developed. A diagram of the model system is displayed below in **Figure 1.8.** First, the photosensitive semiconductor nanomaterials will be illuminated with light at a wavelength of 532 nm, which excites an electron from the valence band into the conduction band. Next, the nanomaterials will bind to Fd and the excited electron from the conduction band will reduce it, initializing electron confurcation. Reduced Fd and NADH bound to HydABCSL will perform a two-electron reduction of FMN, the bifurcating cofactor, which will send electrons down the enzyme's [Fe-S] cluster chain to eventually reduce protons to $H_2$ gas at the [NiFe] active site.

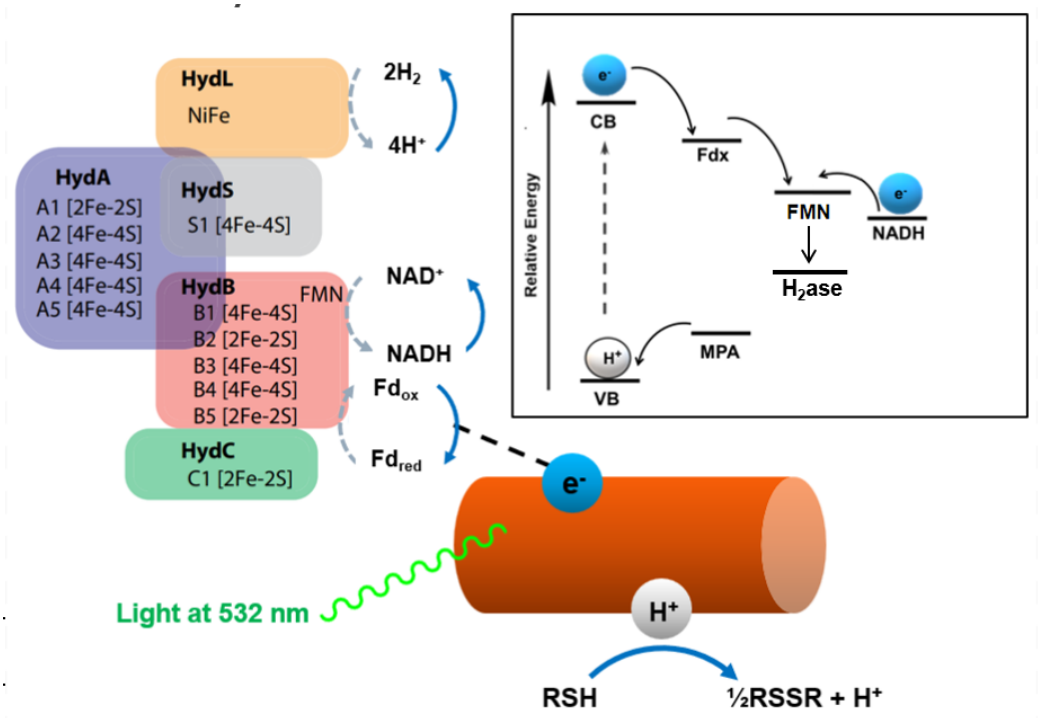


**Figure 1.8** *Amo* Hyd-ABCSL model system for studying light-driven electron confurcation [13]

## 1.5 Scope and Aims

The goal of this work is to develop a photocatalytic system that couples semiconductor nanomaterials with bifurcating *A. mobile* HydABCSL to gain new insights into its mechanism and employ it for artificial photosynthesis. Our first specific aim is to engineer efficient semiconductor nanomaterials that are compatible with the enzyme. A second aim is to

demonstrate light-driven reduction of Fd by the nanomaterials. Finally, this project's primary aim is to find optimal conditions for efficient $H_2$ production via electron confurcation. The overarching objective is to use the optimized system to learn about the mechanism of electron confurcation in *A. mobile* HydABCSL.

### 1.6 References


1. Olabi, A. G.; Abdelkareem, M. Renewable energy and climate change. *Renewable and Sustainable Energy Reviews*. **2022,** *158*, 112111.

2. Haines, A.; Patz, J. A. Health effects of climate change. *JAMA*. **2004**, *1*(291), 99-103.

3. U.S. Energy Information Administration. *Monthly Energy Review*, Table 1.2. **2021**.

4. IEA (2022), *Solar PV*, IEA, Paris https://www.iea.org/reports/solar-pv

5. Joskow, P. Comparing the Costs of Intermittent and Dispatchable Electricity Generating Technologies. *The American Economic Review*. **2011**, *101*(3), 238-241.

6. Jones-Albetus, B. Confronting the Duck Curve: How to Address Over-Generation of Solar Energy. **2017**. https://www.energy.gov/eere/articles/confronting-duck-curve-how-address-over-generation-solar-energy

7. Emmanuel, M; Ramesh, R. Evolution of dispatchable photovoltaic system integration with the electric power network for smart grid applications: A review. *Renewable and Sustainable Energy Reviews*. **2017**, *67*, 207-224.

8. Youvan, D.; Marrs, B. Molecular Mechanisms of Photosynthesis. *Scientific American*. **1987**, *256*(6), 42-49.

9. Felseghi, R.; Carcadea, E.; Raboaca, M.; Trufin, C.; Filote, C. Hydrogen Fuel Cell Technology for the Sustainable Future of Stationary Applications. *Energies*, **2019**, *12*(23), 45-93.

10. Bachmeier, A.; Armstrong, F. Solar-driven proton and carbon dioxide reduction to fuels — lessons from metalloenzymes. *Curr. Opin. Chem. Biol.* **2015**, *25*, 141-151.

11. Mulder, D. W.; Shepard, E. M.; Meuser, J. E.; Joshi, N.; King, P.; Posewitz, M.; Broderick, J.; Peters, J. Insights into [FeFe]-Hydrogenase Structure, Mechanism, and Maturation. *Structure*, **2011,** *19*(8), 1038-1052.

12. Adams, M.; Mortenson, L.; Chen, J. Hydrogenase. *BBA*. **1980,** *594*(2-3), 105-176.

13. Reisner, E.; Powell, D.; Cavazza, C.; Fontecilla-Camps, J.; Armstrong, F. Visible Light-Driven H2 Production by Hydrogenases Attached to Dye-Sensitized TiO2 Nanoparticles. *J. Am. Chem. Soc.* **2009**, *131*(51), 18457-18466.

14. Brown, K.; Wilker, M.; Boehm, M.; Dukovic, G.; King, P. Characterization of Photochemical Processes for H2 Production by CdS Nanorod–[FeFe] Hydrogenase Complexes. *J. Am. Chem. Soc.* **2012**, *134*(12), 5627-5636.

15. Bac*Dive*: doi: 10.1093/nar/gkab961

16. Feng, X.; Schut, G.; Haja, D.; Adams, M.; Huilin, L. Structure and electron transfer pathways of an electron-bifurcating NiFe-hydrogenase. *Sci. Adv.* **2022**, *8*(8).

17. Vaissier, V.; Voorhis, T. Quantum chemical approaches to [NiFe] hydrogenase. *Essays in Biochemistry*, **2017**, *61*, 293-303.

18. Furlan, C.; Chongdar, N.; Gupta, P.; Lubitz, W.; Ogata, H.; Blaza, J.; Birrell, J. Structural insight on the mechanism of an electron-bifurcating [FeFe] hydrogenase. *eLife*, **2022**, *11*.

19. Peters, J.; Miller, A.; Jones, A.; King, P.; Adams, M. Electron bifurcation. *Curr. Opin. Chem. Biol.* **2016**, *31*, 146-152.

20. Yuly, J.; Zhang, P.; Ru, X.; Terai, K.; Singh, N.; Beratan, D. Efficient and reversible electron bifurcation with either normal or inverted potentials at the bifurcating cofactor. *Chem*, **2021**, *7*(7), 1870-1886.

21. Moser, C.; Farid, T.; Chobot, S.; Dutton, P. Electron tunneling chains of mitochondria. *BBA - Bioenergetics*, **2006**, *1757*(9), 1096-1109.

# Chapter 2: Designing and Characterizing Semiconductor Nanomaterials

## 2.1 Introduction

The objective of this chapter is to describe the rationale behind the development of semiconductor nanocrystals used to excite the hydrogenase system, along with their structural characteristics, properties, and efficiency.

Oxidoreductase enzymes, including hydrogenase, may turn over hundreds to thousands of times per second, making their intermediate states very transient and difficult to study spectroscopically. A recently developed method that makes it possible to study oxidoreductase enzyme mechanisms on a sub-turnover timescale uses laser-induced solution potential jumps. This is a general method in which semiconductor nanocrystals are incorporated in solution with the enzyme and are illuminated. When excited with light, an electron from the nanocrystal's valence band jumps into its conduction band, leaving behind a positively charged hole. The excited electron and hole together form a quasiparticle called an exciton, until the hole is filled by a ligand donor on the nanomaterial surface and the electron is transferred to the enzyme, driving turnover. Laser-induced potential jumps have previously been used to spectroscopically study kinetics and intermediate states in [NiFe]- and [FeFe]-hydrogenases, making it an ideal method for studying electron bifurcation in *A. mobile* bifurcating [NiFe]-hydrogenase [1].

To being, several criteria for effective nanomaterials were identified. The first important consideration stems from the use of UV-Visible spectroscopy to track the flow of electrons through the hydrogenase system. Both electron acceptors in the confurcation reaction, FMN and Fd, undergo a color change when reduced. As such, a strong absorbance decay can be seen at 450 nm and 425 nm upon reduction of FMN and Fd, respectively [2,3]. To avoid obscuring this absorbance change in a UV-Vis spectrum, it is important that the nanomaterials do not absorb strongly around the 425-450 nm wavelength range **(Figure 2.1)**. On the other hand, the available laser diode for photoexciting the system emits light with a wavelength of 532 nm, so the nanomaterials must absorb strongly in this region. These considerations indicate the necessity of nanomaterials with an easily tunable absorbance profile. Additionally, the nanomaterials must be stable at pHs suitable for hydrogenase and must be able to electrostatically bind to ferredoxin and efficiently transfer electrons.

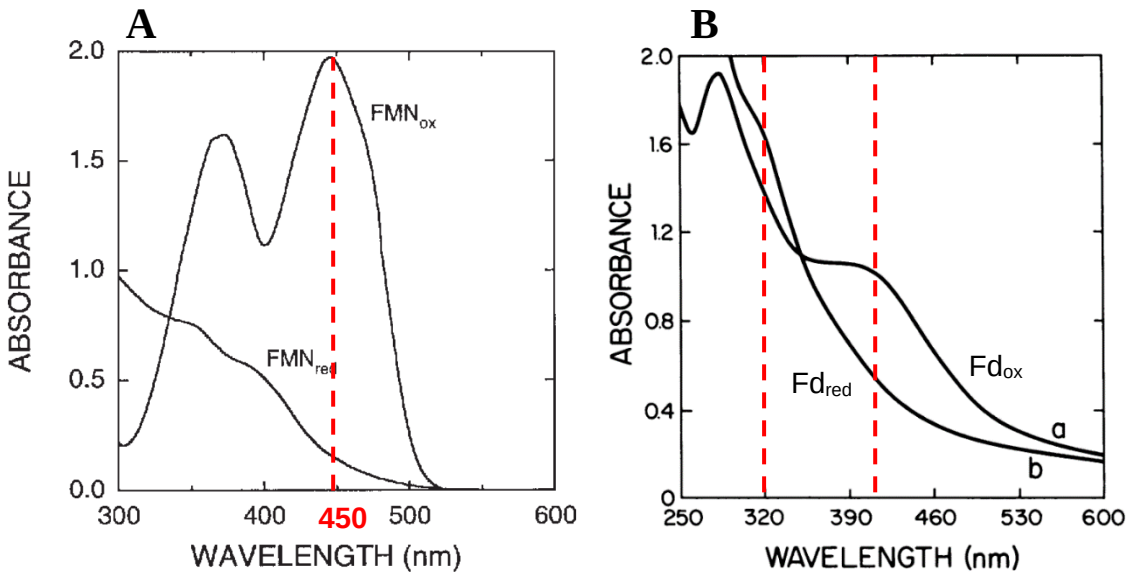


**Figure 2.1.** Change in UV-Visible absorbance spectrum of upon reduction of **(A)** FMN and **(B)** *Pyrococcus furiosus* ferredoxin [2,3]

Colloidal quantum dots are versatile semiconductor nanomaterials with diameters between 2 and 15 nm. Their applications are numerous and varied, including photovoltaics, biological labeling, and quantum dot-based displays [4]. They are particularly useful because they exhibit unique optical and energetic properties due to quantum size effects. Analogously to a particle in a 1D infinite potential, the exciton is confined within the quantum dot, which leads to quantized energy levels. Thus, the properties of quantum dots are size-dependent and can be tuned in a controllable manner [5]. Furthermore, quantum dots can be biocompatible, interacting electrostatically with positively charged protein subdomains due to their negatively charged surface ligands [6]. Collectively, these useful properties make quantum dots suitable candidates that meet the criteria called for. As such, CdSe quantum dots (QDs) and CdSe/CdS quantum dot-in-rods were selected as target nanomaterials for this study. The quantum dot-in-rods (DIRs) consist of a CdSe core with a CdS shell grown over it epitaxially to increase their quantum yield by preventing non-radiative surface recombination of electron-hole pairs [**Berends, Rabouw**].

In the standard synthesis of QDs and DIRs, they are prepared in a nonpolar solvent with hydrophobic ligands. To ensure their solubility in biological buffers and ability to interact with proteins, it is necessary to exchange their surface ligands with polar molecules [8]. Thus, to facilitate electrostatic binding of the nanomaterials to the positively charged binding site of Fd, 3-mercaptopropionic acid (MPA), a three-carbon chain with carboxylic acid and thiol groups,

was selected as the target capping ligand for the QDs and DIRs **(Figure 2.2B)**. MPA covalently binds to the nanomaterials through a sulfur bond, and it stabilizes the quantum dots, ensures their solubility, and drives the nanomaterial-enzyme electron transfer by donating an electron to fill the positively charged hole of the exciton. Upon donating an electron, the MPA molecule detaches from the QD by forming a disulfide bond. Excess MPA in the reaction buffer replaces the original MPA molecule, enabling the process to repeat.

## 2.2 Methodology

Several batches of CdSe QDs and CdSe/CdS DIRs with MPA capping ligands were synthesized, characterized, and evaluated for their compatibility with Fd. A standard synthesis procedure developed by Monica Sanchez at Emory University was followed [9]. Seth Wiley and David White at Emory University also contributed several batches of nanomaterials that were similarly synthesized and evaluated.

### *2.2.1 CdSe Quantum Dot Synthesis*

To begin, 0.06 g cadmium oxide (CdO), 3 g trioctylphosphine oxide (TOPO), and 0.28 g octadecylphosphonic acid (ODPA) were added to a three-neck flask under vacuum, heated to 150°C for 90 minutes, and placed under a nitrogen atmosphere. To fully dissolve the cadmium, the flask was heated again to 350°C until the solution turned transparent. Then, 1.5 mL of trioctylphosphine (TOP) were injected and a Se precursor of 0.058 g Se dissolved in 0.45 mL TOP was also added once the solution's temperature returned to about ~350°C. A rapid color change from clear to orange was observed, and the reaction vessel was removed from the hot plate after several minutes when it turned a deep red-orange color.

### *2.2.2 CdSe/CdS Quantum Dot-in-Rod Synthesis*

A CdS shell was grown around the CdSe quantum dots using a standard procedure from literature [9]. First, 0.06 g CdO, 3 g TOPO, and 0.08 g hexylphosphonic acid were combined in a three-neck flask, heated to 150°C under a vacuum for about two hours, and subsequently placed under a nitrogen atmosphere. After heating the flask to 350°C and attaining a transparent solution indicative of fully dissolved Cd, 1.5 mL TOP was injected into the reaction vessel. Next, a sulfur precursor of 0.12 g S dissolved in 1.5 mL TOP with 2-3 mg of precipitated CdSe quantum dots was injected into the solution. The vessel was reheated to ~350°C, and a color

change to light yellow and increase in fluorescence was observed. The vessel was removed from the hot plate after about five minutes of reaction and mixed with hexanes to keep the nanomaterials in solution phase.

To purify the nanomaterials from unreacted ligands and cadmium, they were centrifuged in methanol to form a precipitate which was resuspended in chloroform. Three to five washes were performed.

### 2.2.3 *Ligand Exchange*

To exchange the nonpolar ligands on the nanomaterials with MPA ligands, the precipitated nanomaterials were dissolved in 15 mL methanol and 10 mM MPA solution. Tetramethyl ammonium hydroxide was used to raise the pH of the solution to at least 10, and it was refluxed under a nitrogen atmosphere for about two hours. The ligand-exchanged quantum dots were purified with centrifugation and stored in a buffer of 10 mM MPA, 10 mM triscarboxyethyl phosphide and 50 mM borate buffer in an anaerobic, light-free glovebox.

### *2.2.4 Nanomaterial Characterization and Quantum Efficiency*

Before the ligand exchange procedure, one drop of the CdS/CdSe DIRs was transferred to a TEM grid which was imaged using a standard transmission electron microscope. Additionally, a UV-Visible absorbance spectrum of both the QDs and DIRs was taken and demonstrates the shift in the absorption profile caused by the growth of the CdS shell.

Next, the ability of the QDs/DIRs to convert absorbed photons to excited electrons was evaluated by measuring their quantum yield. Quantum yield is a ratio of the moles of radical produced when the QDs/DIRs reduce a species in solution to the moles of photons they absorb, and it indicates the efficiency of the nanomaterials as semiconductors [10]. Specifically, we evaluated quantum yield using an organic redox mediator dye DQ03 that the DIRs reduce upon illumination with 532 nm wavelength light. DQ03 has a redox potential of -550 mV and is colorless until reduced to form an intensely colored radical, making it easy to track with UV-Visible spectroscopy [11]. The setup of the quantum yield experiments is displayed in **Figure 2A**.

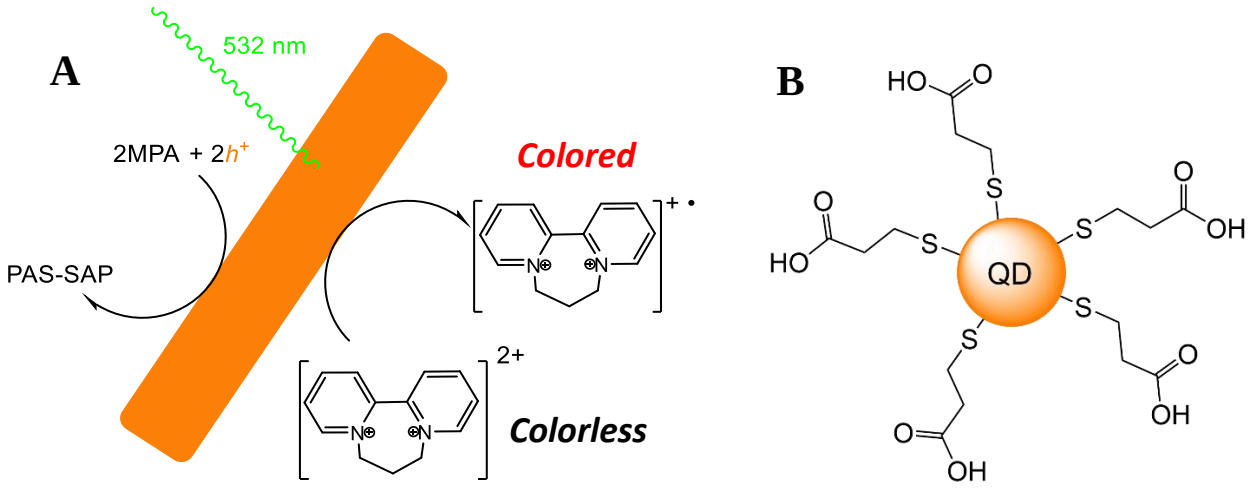


**Figure 2.2 (A)** Set up for measuring the quantum yield of the nanomaterials. **(B)** MPA ligands.

The storage buffer of the DIRs was exchanged with a pH 8 reaction buffer of 100 mM MPA and 50 mM potassium phosphate, the standard reaction buffer that we use for all experiments in this thesis. Next, a cuvette containing the DIRs and DQ03 was illuminated while tracking absorbance changes, and Equation 1 was used to calculate a quantum yield.

$$QY = \frac{moles\ of\ radical}{laser\ power \times photons \times \%\ photons\ absorbed \times (1 - scatter) \times \frac{1}{N_A}}$$

**Equation 1.** Quantum yield of nanomaterials where $N_A$ is Avogadro's number [10]

### *2.2.5 Steady-State Photoreduction of Ferredoxin*

The objective of the nanomaterials is to efficiently convert absorbed photons to electrons that can reduce Fd, which has a redox potential of about -400 mV [12]. As such, once it was determined that the nanomaterials were sufficiently efficient with DQ03, an experiment was performed to determine what percent of oxidized *P. furiosus* and *A. mobile* Fd the nanomaterials were able to reduce in one hour.

As before, the DIR storage buffer and original Fd buffer were exchanged with a pH 8 reaction buffer with 100 mM MPA and 50 mM potassium phosphate in a glovebox. A cuvette containing 0.2-0.3 OD QDs/DIRs and either 100 uM *Pfu* or 25 uM *Amo* Fd was illuminated by laser light of wavelength 532 nm. The solution was stirred throughout the experiment, and

absorbance changes were tracked at 425 nm using UV-Visible spectroscopy over the course of approximately one hour.

## 2.3 Results and Discussion

### *2.3.1 Characterization of Nanomaterials*

Each batch of QDs and DIRs had unique absorbance profiles and quantum yields, despite being synthesized in the same way. Overall, the shelled DIRs were substantially more fluorescent than the QDs. The DIRs were very homogeneous, forming uniform rod-like shapes that were approximately 20 nm long. Additionally, the second maximum peak of the quantum dots shifted to a higher wavelength and lower intensity when they were shelled, although their quantum yields generally increased **(Figure 2.3)**.

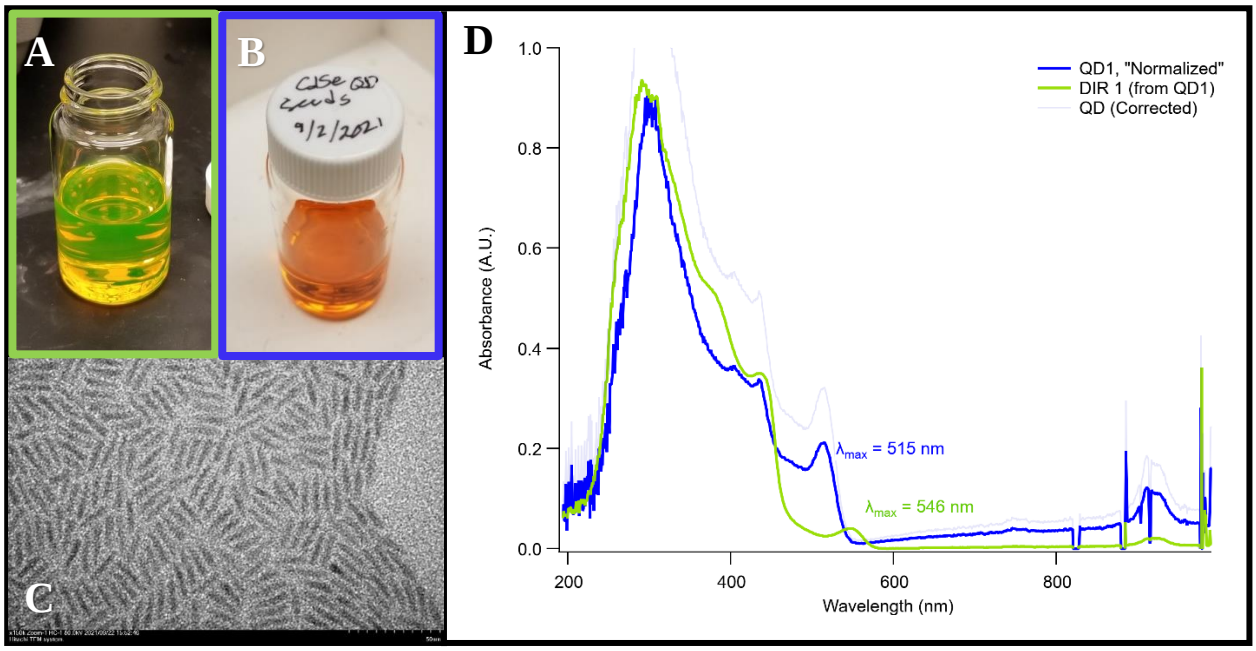


**Figure 2.3. (A)** CdSe dot-in-rods are highly fluorescent after being shelled with CdS. (B) CdSe quantum dots turned an orange-red color. **(**C) TEM image of CdSe/CdS DIRs shows their uniformity and ~20 nm length. (D) The wavelength of the laser light-absorbing peak shifts from 515 nm for QDs to 546 nm for DIRs.

The quantum yields for most nanomaterials were around 30-60%, which are typical ratios for CdSe-based quantum dots. For reference, the quantum yields for other types of surface-passivated quantum dots are 65-85% for CdSe, 10-40% for InP, and 30-75% for CdTe, all of

which are comparable to the observed yields [13]. Although the shelled DIRs had higher quantum efficiencies than the QDs, they had a lower absorbance in the 532 nm region, requiring higher concentrations to reach an OD of 0.2-0.3. The DIRs were also more time- and resource-intensive to synthesize than the QDs with variable levels of success. For instance, DIR 3 formed heterogeneous and asymmetric rods presumably due to the addition of too much CdS precursor, and these nanomaterials had a quantum yield that was not substantially better than the QDs and lacked an absorbance peak around 532 nm. As such, QDs were used for most subsequent experiments.

**Table 2.1** Quantum efficiencies with DQ03 and $\lambda_{max}$ of nanomaterials used in study.

| **Nanomaterial ID** | **Laser Wavelength (nm)** | **Quantum efficiency** | **λ of Relevant Peak (nm)** |
|---|---|---|---|
| DIR 1 | 532 | 63% | 547 |
| DIR 3 | 450 | 39% | 466 (shoulder) |
| QD3* | 532 | 32% | 587 |
| QD7** | 532 | 65% | 538 |
| DIR12* | 532 | 54% | 584 |
| DIR 13* | 532 | 97% | 566 |

*synthesized by Seth Wiley, **synthesized by David White

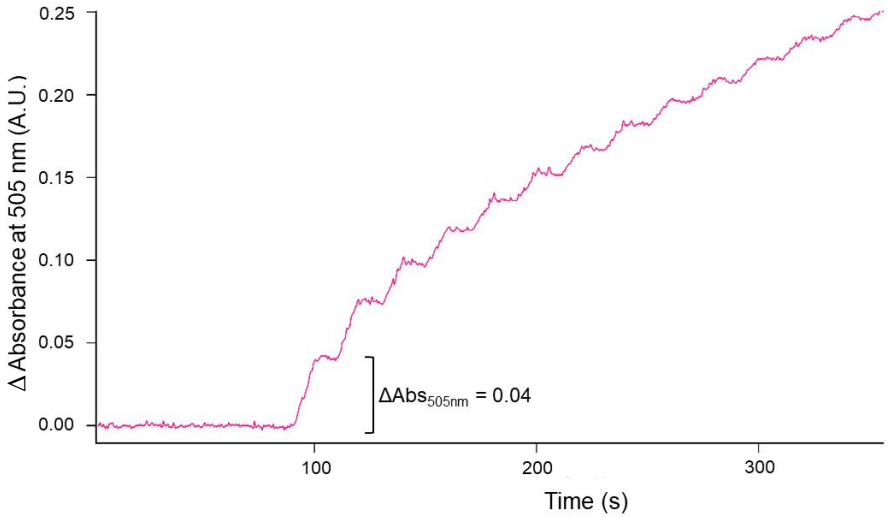


**Figure 2.4.** Light-induced potential jump of DIR 1 used to calculate quantum efficiency by measuring absorbance change at λ=505 nm, which indicates the amount of DQ03 radical in solution.

The ability of the nanomaterials to efficiently reduce DQ03 is an encouraging sign of their potential ability to reduce ferredoxin. The redox potential of DQ03 is -550 mV and is higher than that of most ferredoxins which is around -400 mV [12]. A more positive reduction potential means that a species has a greater tendency to get reduced, so if the QDs can electrostatically bind to Fd, they should be able to reduce it.

*2.3.2 Steady-State Photoreduction of Ferredoxin*

Successful binding and reduction of *Pfu* Fd by QD 7 was observed, as is evident from the decrease in absorbance around 425 nm shown in **Figure 2.5A**. It took about an hour to achieve an equilibrium steady-state concentration of reduced Fd, as demonstrated by the eventual plateau of the absorbance change at 425 nm which corresponds to an increase in the concentration of $Fd_{red}$ (**Figure 2.5B**). Using a molar extinction coefficient of $\epsilon_{390}$=27,000 $M^{-1}cm^{-1}$ for oxidized Fd [14] and $\epsilon_{425}$=13,000 $M^{-1}cm^{-1}$ for reduced Fd, [15] it was determined that approximately 70% of the original Fd was reduced by the nanomaterials after 50 minutes.

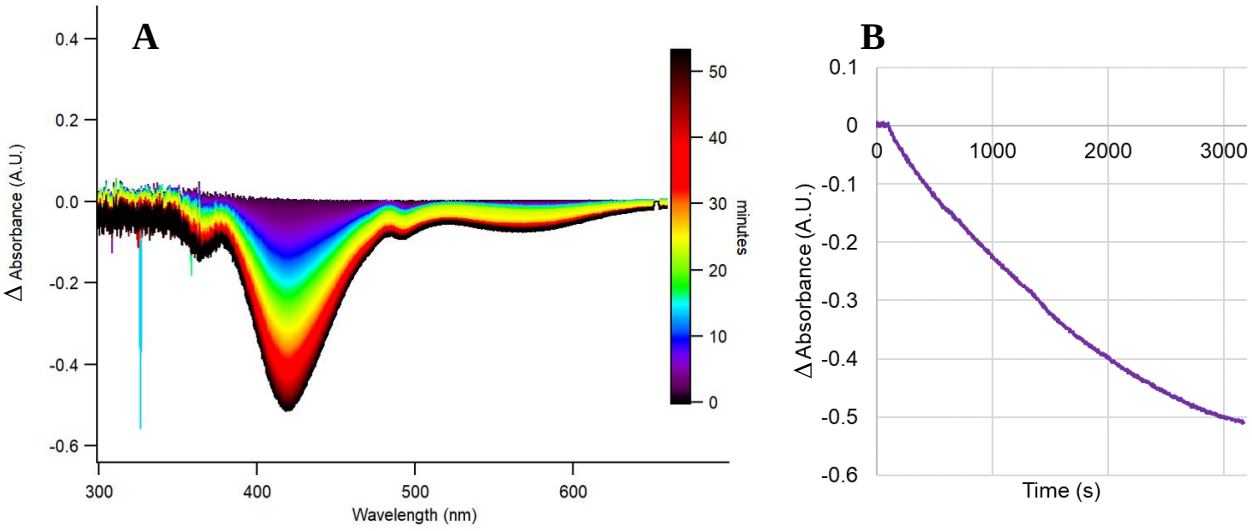


**Figure 2.5 (A)** Absorbance changes indicate photoreduction of 100uM *Pfu* Fd by QD 7 **(B)** Concentration of reduced *Pfu* Fd stabilizes after 50 minutes, implying that the system has reached a steady-state equilibrium.

Similar results were observed when using QD 3 to reduce *Amo* Fd. The decrease in absorbance at 425 nm indicates *Amo* Fd reduction (**Figure 2.6A**), and this reaction also reached a

steady-state equilibrium reduced Fd concentration after approximately one hour, as shown by the eventual plateau in Fd reduction rate in **Figure 2.6B**. Roughly 20% of the original concentration of *Amo* $Fd_{ox}$ was reduced, which was calculated using the same molar extinction coefficients reported previously and assuming that all Fd added to the system began in its oxidized form.

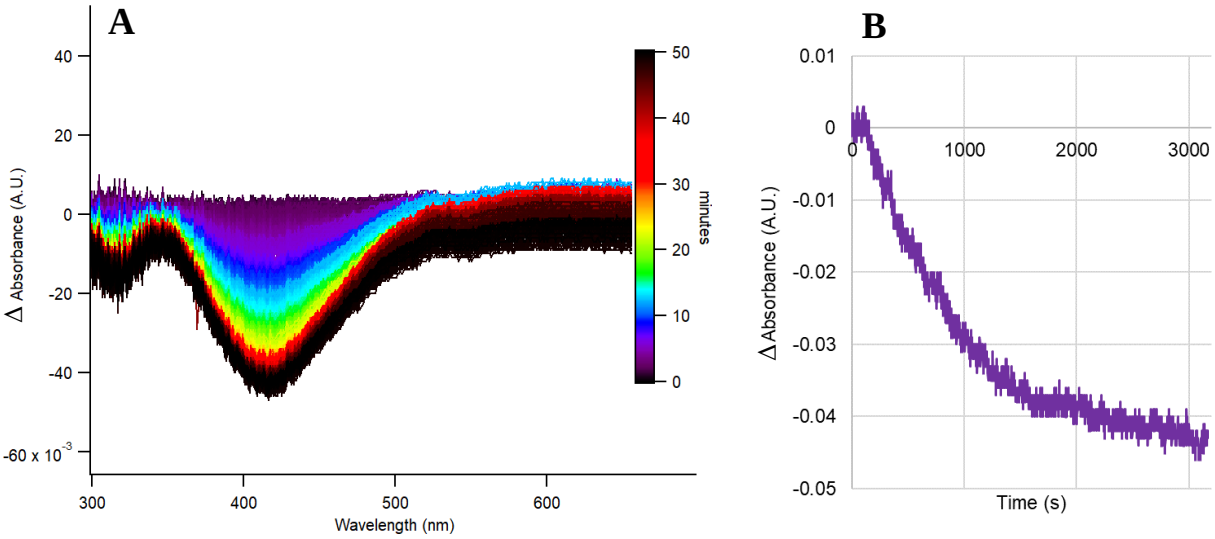


**Figure 2.6 (A)** Absorbance changes indicate successful photoreduction of 25 uM *Amo* Fd by QD 3 **(B)** Concentration of reduced *Amo* Fd stabilizes after 60 minutes, implying that the system has reached a steady-state equilibrium.

The lower ratio of *Amo* $Fd_{red}$:$Fd_{ox}$ compared to *Pfu* $Fd_{red}$:$Fd_{ox}$ at equilibrium may be thought to be a result of the lower quantum yield of QD 3 (QY=32%) used to reduce *Amo* Fd compared to that of QD 7 (QY=65%) used to reduce *Pfu* Fd. Since QD 3 is about half as efficient as QD 7, it should take about twice as long to obtain the same level of Fd reduction. However, the kinetics of both reactions appear to follow similar trajectories, reaching an equilibrium after approximately 60 minutes of reaction time. An alternative explanation for the contrasting ratios of $Fd_{red}$:$Fd_{ox}$ at equilibrium is that the two species of Fd may have different reduction potentials, resulting in one species favoring $Fd_{red}$ more than the other. This would be in line with the general observation that [FeFe]-hydrogenases like that from *Pfu* tend to prefer hydrogen production and thus Fd reduction more than [NiFe]-hydrogenases like that from *Amo*. It is also possible that electrostatic binding of the nanomaterials to *Amo* Fd is more difficult than binding to *Pfu* Fd because of differences in surface charge or structure, which could also contribute to the reduced proportion of $Fd_{red}$ at equilibrium.

Overall, these experiments indicate that the QDs synthesized appear to be optimal for the system and meet all the proposed criteria – possessing a high quantum yield and affinity for both *Pfu* and *Amo* Fd, and not blocking out UV-Visible absorbance signals in the 425-450 nm range.

**References**


1. Sanchez, M.; Konececny, S.; Narehood, S.; Reijerse, E.; Lubitz, W.; Birrell, J.; Dyer, B. The Laser-Induced Potential Jump: A Method for Rapid Electron Injection into Oxidoreductase Enzymes. *J. Phys. Chem.* **2020**, *40*, 8750-8760.

2. Macheroux, P. UV-Visible Spectroscopy as a Tool to Study Flavoproteins. *Methods in molecular biology*. **1999**, *131*, https://doi.org/10.1385/1-59259-266-X:1

3. Wang, S.; Huang, H.; Kahnt, J.; Thauer, R. A Reversible Electron-Bifurcating Ferredoxin- and NAD-Dependent [FeFe]-Hydrogenase (HydABC) in *Moorella thermoacetica*. **2013**, *195*, 1267-1275.

4. Cotta, M. Quantum Dots and Their Applications: What Lies Ahead? *ACS Applied Nano Materials*. **2020**. *3*(6). 4920-4924.

5. Alivisatos, P. Perspectives on the Physical Chemistry of Semiconductor Nanocrystals. *J. Phys. Chem.* **1996**, *100*(31), 13226-13239.

6. Ratnesh, R. K.; Mehata, M. S. Investigation of biocompatible and protein sensitive highly luminescent quantum dots/nanocrystals of CdSe, CdSe/ZnS and CdSe/CdS. *SAA.* **2017**, *179*, 201-210.

7. Berends, A.; Rabuow, F.; Spoor, F.; Bladt, E.; Grozema, F.; Houtepen, A.; Siebbeles, L.; de Mello Donega, C. Radiative and Nonradiative Recombination in CuInS2 Nanocrystals and CuInS2-Based Core/Shell Nanocrystals. *J. Phys. Chem. Lett.* **2016**, *7*(17), 3503-3509. **(new 7)**

8. Zhang, Y.; Clapp, A. Overview of Stabilizing Ligands for Biocompatible Quantum Dot Nanocrystals. *Sensors*. **2011**, *11*(12), 11036-11055.

9. Sanchez, M.; Sommer, C.; Reijerse, E.; Birrell, J.; Lubitz, W.; Dyer, B. Investigating the Kinetic Competency of *Cr*HydA1 [FeFe] Hydrogenase Intermediate States via Time-resolved Infrared Spectroscopy. *JACS.* **2019,** *141*(40), 16064-16067.

10. Chica, B.; Wu, C.; Liu, Y.; Adams, M.; Lian, T.; Dyer, B. Balancing electron transfer rate and driving force for efficient photocatalytic hydrogen production in CdSe/CdS nanorod–[NiFe] hydrogenase assemblies. *Energy Environ. Sci.* **2017,** *10*(10), 2245-2255.

11. Sanchez, M.; Wu, C.; Adams, M.; Dyer, B. Optimizing electron transfer from CdSe QDs to hydrogenase for photocatalytic H2 production. *ChemComm*. **2019,** *55*(39), 5579-5582.

12. Maiocco, S.; Arcinas, A.; Booker, S.; Elliott, S. Parsing redox potentials of five ferredoxins found within *Thermotoga maritima*. *Protein Sci.* **2019,** *28*(1), 257-266.

13. Grabolle, M.; Spieles, M.; Lesnyak, V.; Gaponik, N.; Eychmuller, A.; Resch-Genger, U. Determination of the Fluorescence Quantum Yield of Quantum Dots: Suitable Procedures and Achievable Uncertainties. *Anal. Chem.* **2009,** *81*(15), 6285-6294.

14. Aono, S.; Bryant, F.; Adams, M. A. A novel and remarkably thermostable ferredoxin from the hyperthermophilic archaebacterium *Pyrococcus furiosus*. *J. Bacteriol.* **1989,** *171*(6), 3433-3439.

15. Tagawa, K.; Arnon, D. Oxidation-reduction potentials and stoichiometry of electron transfer in ferredoxins. *BBA.* **1968,** *153*(3), 602-613.

## Chapter 3: Optimizing Conditions for Light-Driven Hydrogen Production

### 3.1 Introduction

The goal of this chapter is to describe the steps taken to optimize various parameters of the hydrogenase system, including cofactor concentrations, temperature, ferredoxin species, and type of nanomaterials used. The ability to successfully drive electron confurcation with light is evaluated and takeaways about the electron confurcation mechanism employed by *A. mobile* HydABCSL are discussed.

Light-driven electron confurcation in *Amo* hydrogenase is complex, involving numerous conformational changes, thermodynamically challenging electron transfers, and an unhindered electron transport chain through a series of [Fe-S] clusters to the protein's active site [1]. Quantification of electron confurcation is also challenging. Although FMN and Fd undergo color changes when reduced, the concentration of FMN used in our experiments was not large enough to be registered by UV-Visible spectroscopy. Thus, the rate of pressure production was used as the primary metric for evaluating electron confurcation. Although hydrogenase enzymes can produce hydrogen in the presence of a single electron donor – whether Fd, NADH, or another reducing species that binds to hydrogenase near an [Fe-S] cluster – the rate of $H_2$ production is substantially faster via electron confurcation [1].

To determine a threshold rate of hydrogen production that corresponds to electron confurcation, we turned to literature. We found that a hydrogen production assay using 70 ug *Amo* NiFe-HydABCSL enzyme, 10 uM FMN, 1mM NADH, 10uM *Amo* Fd that was reduced by *Amo* pyruvate Fd oxidoreductase, alongside several additional cofactors led to clear signs of electron confurcation indicated by the rate of $H_2$ production. Minimal $H_2$ production was observed if only Fd or NADH were present, but significant $H_2$ was generated at a rate of 2 nmol $H_2$/mg protein in the presence of both Fd and NADH – presumably indicating that the enzyme was utilizing electron confurcation (**Figure 3.1**). Since we used similar reaction conditions in our experiments, we take the pressure production rate of 2 nmol $H_2$/mg protein/min to be the threshold that indicates successful electron confurcation and functioning of the system.

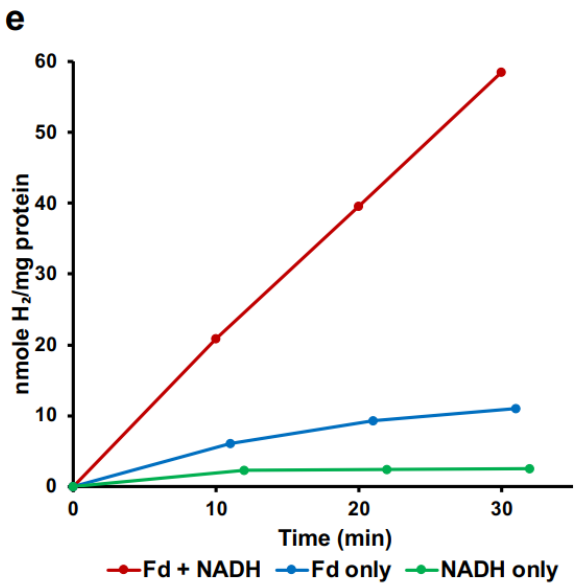


**Figure 3.1** Evidence of electron confurcation in *Amo* NiFe-HydABCSL by increase in pressure production rate when both Fd and NADH are present in the reaction [1].

## 3.2 Methodology

All enzymes used, including all ferredoxin and hydrogenase proteins, were prepared and purified at the University of Georgia Department of Biochemistry and Molecular Biology in the laboratory of Dr. Michael Adams. Proteins were stored in a -80°C freezer once they were received, and special care was taken to avoid oxygen exposure.

### *3.2.1 Hydrogenase Activity Assay*

To confirm that the *Amo* hydrogenase sample was active, an oxidation assay was performed following a procedure from literature [1]. A cuvette with 200 nM *Amo* hydrogenase and 5 mM benzyl viologen in a pH 7.5 Hepes buffer was prepared in an anaerobic glovebox. The cuvette headspace was put under 5% $H_2$ gas, and absorbance changes were tracked over six minutes using an Ocean Optics UV-Vis spectrometer. Successful activity is indicated by efficient conversion of hydrogen gas to protons and electrons by the hydrogenase enzyme, which is tracked by reduction of benzyl viologen – a mediator dye that turns a deep purple color when reduced and absorbs light at 600 nm.

*3.2.2 Hydrogen Production Assays*

A series of hydrogen production assays under various conditions served to evaluate the ability of the hydrogenase system to produce $H_2$ gas via electron confurcation. To begin, a buffer exchange of Fd, hydrogenase, and QDs/DIRs was performed in an anaerobic glovebox with a pH 8 buffer of 100 mM MPA and 50 mM potassium phosphate in DI water. Next, 200 nM hydrogenase, 100 uM Fd, 1 mM NADH, 200 nM FMN, and 0.2-0.3 OD QDs/DIRs were mixed in a cuvette. At times, the Fd and hydrogenase concentrations were varied, but the standard conditions are those listed above, optimized by Sarah Narehood at Emory University for light-driven hydrogen production by [FeFe]-hydrogenase from *Thermotoga maritima* [2]. A Phidgets pressure sensor was attached to the cuvette cap, and care was taken to ensure that the cap kept the cuvette airtight. The solution was illuminated by a Thor Labs laser diode with a wavelength of 532 nm while being continuously stirred. An Ocean Optics UV-Visible spectrometer was used to track absorbance changes at 425 nm indicative of Fd reduction, and pressure changes were tracked using a digital sensor attached to the cuvette cap.

Recorded pressure values were converted to nmol $H_2$ using Henry's law, which describes the pressure change that accompanies an increase in the concentration of a gas over a liquid, accounting for dissolved gas in the liquid. Henry's Law is displayed in **Equation 1**, and for $H_2$ gas, a constant of $k = 7.8 \times 10^{-4}\ \frac{mol}{L \bullet atm}$ was used in calculations [3].

$$P = kC$$

**Equation 1.** Henry's law of partial pressure

*3.2.3 Effect of FMN Concentration on Electron Bifurcation Rate*

To assess whether the *Amo* hydrogenase enzyme required reconstitution with FMN, the rate of electron bifurcation before and after addition of excess FMN was determined using an electron bifurcation assay. Inside an anaerobic glovebox, the storage buffer of *Amo* hydrogenase and *Pfu* Fd were exchanged with a pH 8 buffer of 100 mM MPA and 50 mM potassium phosphate dissolved in DI water. Next, 200 nM *Amo* Fd, 100 uM *Pfu* Fd, and 1 mM $NAD^+$ were mixed in a cuvette, which was capped and removed from the glovebox. Subsequently, 5% $H_2$ gas

was injected into the headspace of the cuvette and UV-Visible spectroscopy was used to track changes in absorbance at 425 nm, corresponding to reduction of *Pfu* Fd.

### *3.2.4 Photoluminescence Quenching of CdSe Quantum Dots with Amo Hydrogenase*

To determine the binding behavior of CdSe QDs to *Amo* hydrogenase, a photoluminescence quenching assay was performed. In an anaerobic glovebox, a sample of 0.2-0.3 OD QD 3 was buffer exchanged with a pH 8 solution of 100 mM MPA and 50 mM potassium phosphate and prepared in an airtight cuvette. Using a Horiba Dual FL fluorometer, the cuvette was excited with 532 nm wavelength light and emission spectra were repeatedly recorded as increasing aliquots of *Amo* hydrogenase were injected into the cuvette using an airtight Hamilton syringe.

## 3.3 Results and Discussion

### *3.3.1 Hydrogenase Activity Assays*

Hydrogenase activity assays were performed at 20°C and 50°C, and the full spectrum of absorbance changes for the 20°C assay is displayed in **Figure 3.2A** below. Evidence from both assays showed that the HydABCSL enzyme was highly active, capable of rapidly turning over $H_2$ gas in the cuvette's headspace to electrons that reduced benzyl viologen in solution. The enzyme appeared to be significantly more active at 50°C than at 20°C, reducing benzyl viologen at a ten times faster rate than at the lower temperature as shown in **Figure 3.2B**.

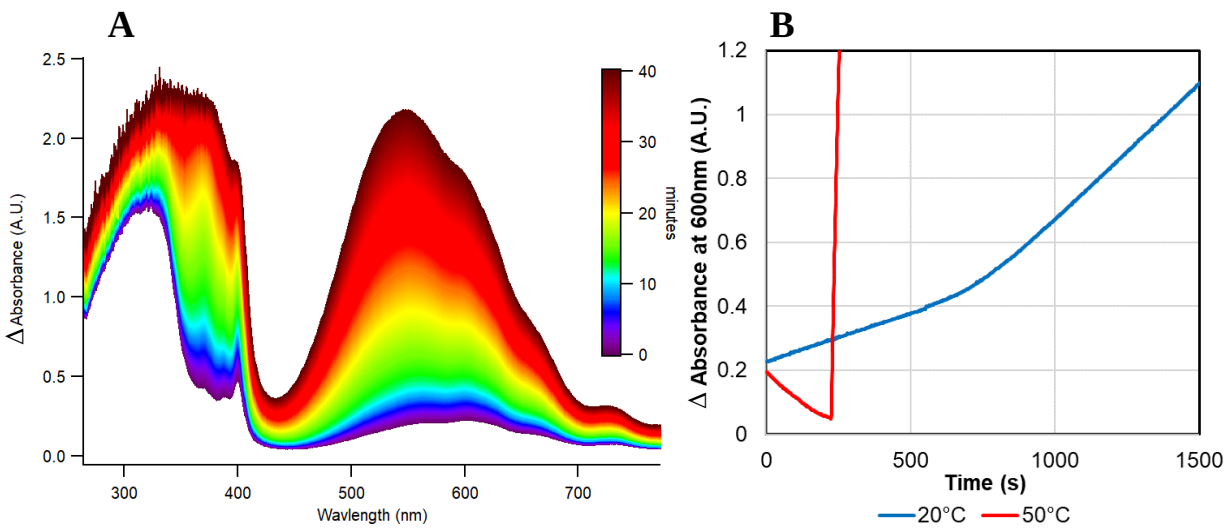


**Figure 3.2** Hydrogenase activity assay with 200 nM *Amo* hydrogenase and 5 mM benzyl viologen: **(A)** Change in full absorbance spectrum over 40 minutes for assay at 20°C. **(B)** Increase in absorbance at 600 nm indicates successful reduction of benzyl viologen and is about ten times faster at 50°C than at 20°C.

This result was anticipated, since *A. mobile* is a thermophilic species that thrives at high temperatures. Although faster turnover is observed at 50°C, these experiments motivated our choice of 25°C for subsequent experiments. The stability and binding constant of CdSe QDs tends to decrease at higher temperatures, so lower temperatures are safest for the system given that *Amo* hydrogenase also functions effectively in this regime [4]. Additionally, pressure was tracked using a sensor that cannot register pressures above 7 kPa, and we determined that the pressure in the cuvette headspace even before $H_2$ production exceeds the maximum detectable limit at 50°C.

### *3.3.2 Hydrogen Production Assays*

Conditions for light-driven electron confurcation in [FeFe]-hydrogenase from *T. maritima* were optimized by Sarah Narehood at Emory University, so a control experiment was performed using the conditions and procedure described in her work [2]. Success of electron bifurcation was quantified by tracking absorbance changes at 425 nm, which correspond to reduction of *Tma* Fd, (**Figure 3.3A**) and the rate of $H_2$ production (**Figure 3.3B**). It was determined that at steady state equilibrium, approximately 17% of the original Fd existed in its reduced form and that the system generated approximately 0.1 nmol of $H_2$ after 80 minutes. This

corresponds to a rate of roughly 2.1 nmol of $H_2$/mg protein/min, which indicates enzyme turnover via an electron confurcation pathway. Thus, this experiment demonstrates the feasibility of driving $H_2$ production with light under the conditions used.

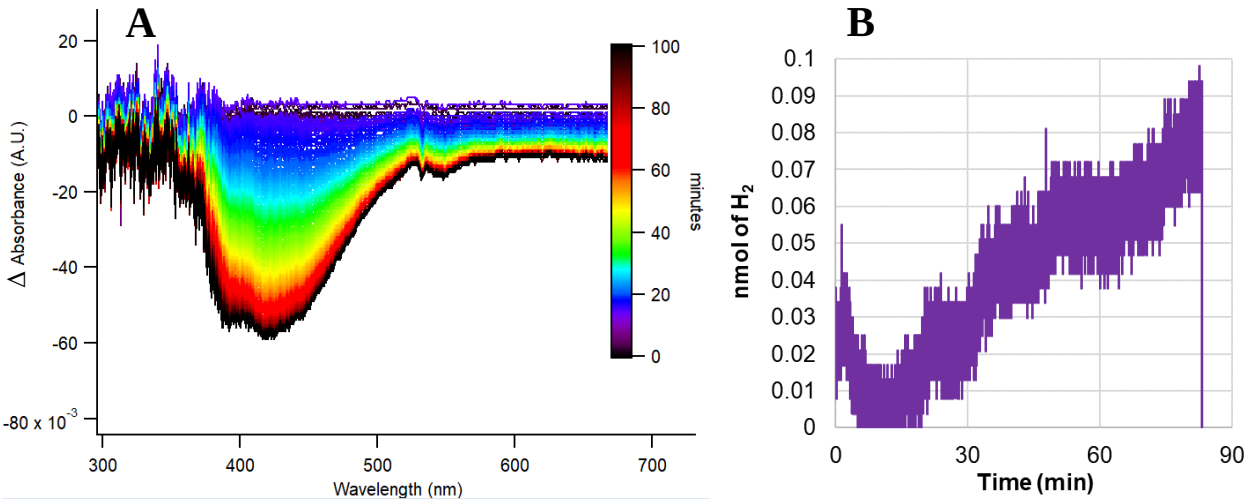


**Figure 3.3 (A)** Hydrogen production assay using *Tma* hydrogenase (0.046 mg) and *Tma* Fd (50 uM) **(B)** Approximately 0.1 nmol of $H_2$ are generated after 80 minutes of illumination.

Next, a hydrogen production assay was conducted using *Amo* hydrogenase and *Pfu* Fd under the same conditions that were sufficient for electron confurcation in *Tma* hydrogenase. Although there appeared to be efficient transfer of electrons from the QDs to Fd, as demonstrated by the 78% decrease in absorbance at 425 nm in **Figure 3.4A**, the rate of $H_2$ production did not show signs of electron confurcation. As shown in **Figure 3.4B**, approximately 0.9 nmol of $H_2$ were generated in one hour, corresponding to a rate of 0.1 nmol $H_2$/mg protein/min. Usually, [FeFe]-hydrogenases are more primed for hydrogen production than [NiFe]-hydrogenases, so the result that *Amo* [NiFe]-hydrogenase requires more extreme conditions than *Tma* [FeFe]-hydrogenase to drive electron confurcation is unsurprising [5].

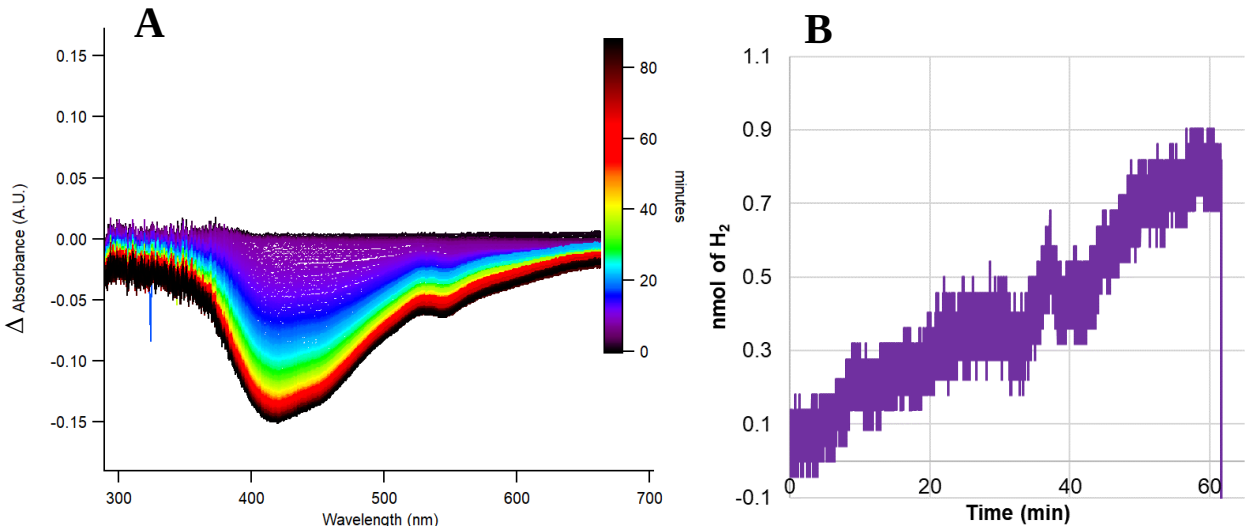


**Figure 3.4 (A)** Absorbance changes at 425 nm during $H_2$ production assay with *Amo* hydrogenase (0.13 mg) and *Pfu* Fd (100 uM) indicate efficient Fd reduction. **(B)** Approximately 6 nmol $H_2$/mg protein were produced after 60 minutes.

In theory, if *Amo* hydrogenase is simply less effective at turning over protons and electrons to hydrogen than *Tma* hydrogenase, then increasing its concentration should similarly increase the amount of $H_2$ generated. Following this line of reasoning, another hydrogen production assay was conducted using the same conditions as in the previous experiment, but with triple the amount of hydrogenase (600 nM *Amo* hydrogenase).

Interestingly, there were approximately 30 umol of reduced Fd at steady state equilibrium, which is about a third of the 78 umol of reduced Fd at equilibrium observed in the previous experiment (**Figure 3.5**). Assuming that Fd transfers electrons to hydrogenase, tripling the concentration of hydrogenase means that there are three times as many electron acceptors for $Fd_{red.}$ Since a decrease in the concentration of $Fd_{red}$ corresponding to the increase in *Amo* hydrogenase was observed in this experiment, this result suggests that *Pfu* Fd successfully transfers electrons to *Amo* hydrogenase – the next step required for electron confurcation.

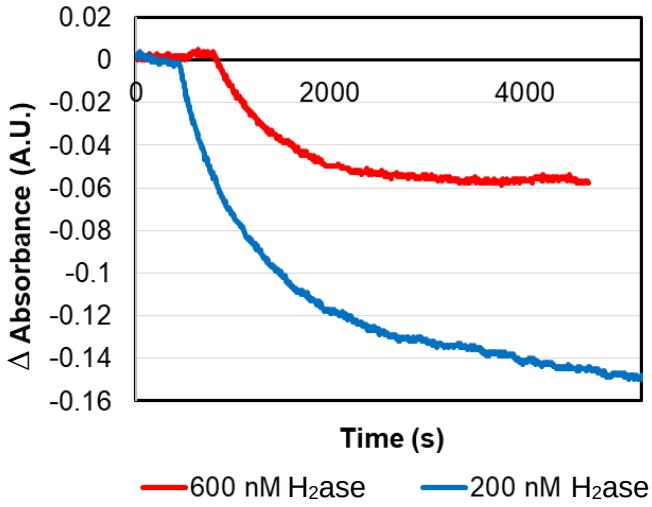


**Figure 3.5** Lower equilibrium concentration of $Fd_{red}$ with 600 nM *Amo* hydrogenase indicates successful electron transfer from *Amo* Fd to *Amo* hydrogenase.

However, the rate of pressure generation did not corroborate the activity of the electron confurcation pathway for $H_2$ generation. In fact, as shown in **Figure 3.6B**, the total amount of $H_2$ generated was roughly equivalent to that observed in the previous experiment (0.8 nmol in 70 minutes vs. 0.9 nmol in 60 minutes). The independence of the rate of $H_2$ generation and the concentration of hydrogenase is a clear sign that there is a rate-limiting step that occurs after electron transfer from Fd to HydABCSL that prevents the electrons transferred to hydrogenase from participating in electron confurcation.

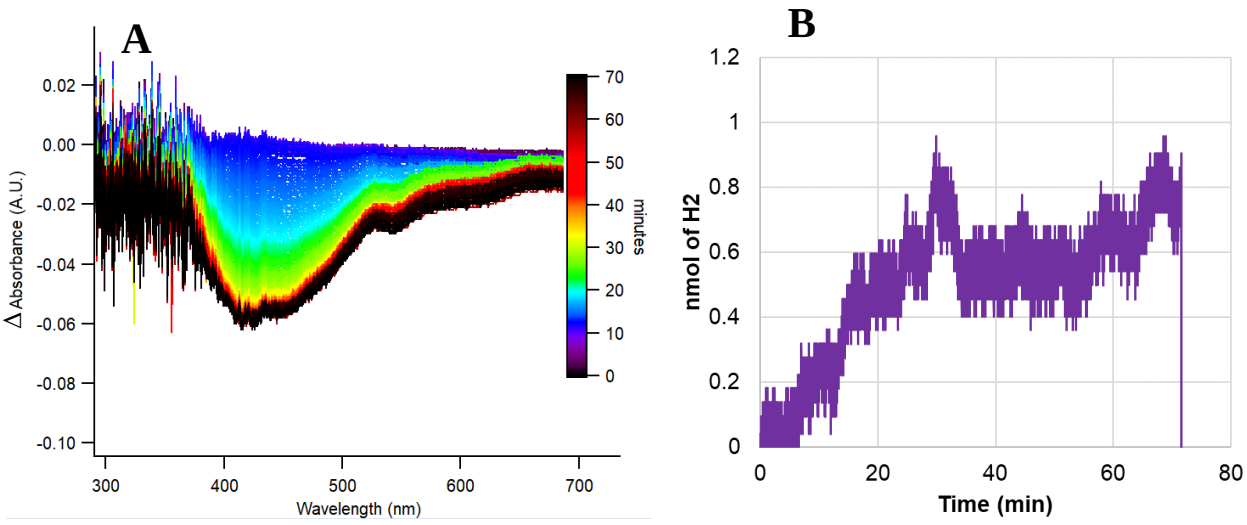


**Figure 3.6 (A)** Absorbance changes during $H_2$ production assay indicate that three times more electrons are being donated by Fd. **(B)** About 0.8 nmol of $H_2$ are produced over 70 minutes.

Circumstantial evidence from cryo-EM data indicates that the mechanism of *Amo* hydrogenase involves conformational changes triggered by binding of cofactors in particular locations on the enzyme [1]. As such, it is possible that the protein is highly specific and cannot function with *Pfu* Fd as a substitute for *Amo* Fd. For instance, *Pfu* Fd could be binding to a site in which it cannot donate its electrons to participate in the bifurcation pathway.

To evaluate this possibility, a hydrogen production assay was performed using *Amo* Fd (25 uM) instead of *Pfu* Fd, otherwise under the same conditions as the original assay. As can be seen in **Figure 3.7A**, the decrease in absorbance at 425 nm indicates successful Fd reduction by the QDs, and the equilibrium concentration of $F_{red}$ was approximately 8 uM. Surprisingly, there was no net $H_2$ production, and the pressure appeared to oscillate randomly throughout the duration of the experiment.

Although we hypothesized that the lack of $H_2$ produced was caused by the low *Amo* Fd concentration, a repetition of this experiment using 50 uM *Amo* Fd also showed no pressure production.

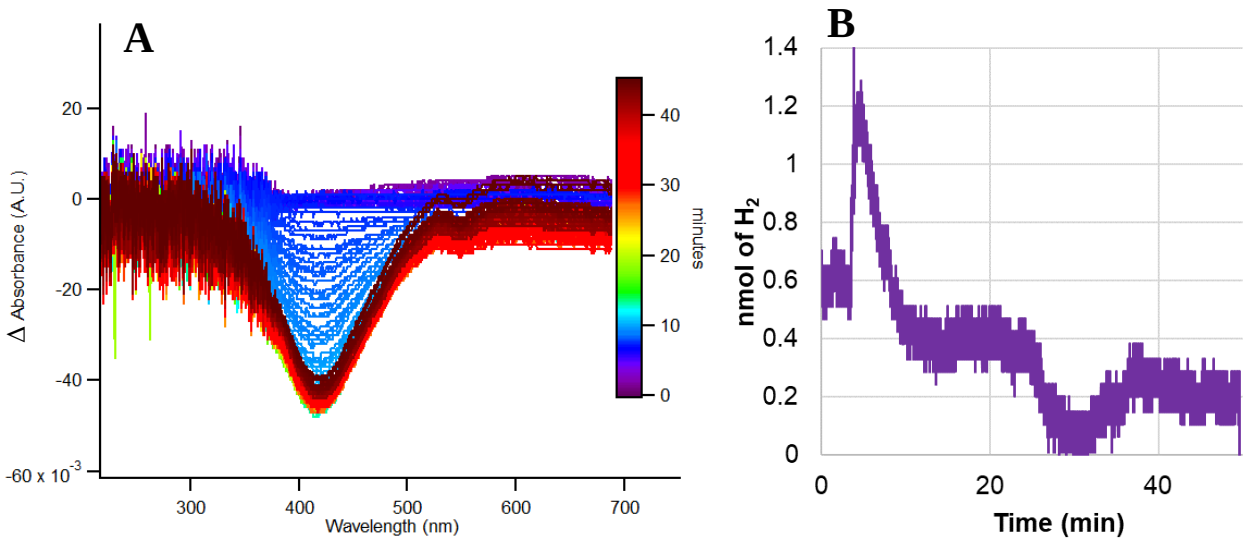


**Figure 3.7 (A)** The 31% absorbance change at 425 nm indicates reduction of Fd during the $H_2$ production assay with *Amo* hydrogenase (200 nM, 0.13 mg) and *Amo* Fd (25 uM). **(B)** No net pressure production was produced over 50 minutes.

*3.3.3 Effect of FMN Concentration on Electron Bifurcation Rate*

As the midpoint acceptor for electrons from Fd and NADH and the bifurcating cofactor for electron confurcation, FMN plays a critical role in enzyme turnover. Since experiments took place over the course of many months, a concern that arose was whether FMN could have fallen out of the enzyme. As such, the rate of electron bifurcation by HydABCSL was measured before and after a large excess of FMN was injected into the reaction vessel, where the enzyme's ability to convert hydrogen gas to electrons was evaluated via reduction of Fd. **Figure 3.8** shows that the rate of Fd reduction was 0.05 Fd/min before FMN injection and 0.08 Fd/min after. The increase in rate is miniscule and likely insignificant, indicating that the amount of FMN bound to the enzyme is sufficient without need of reconstitution and that the enzyme can undergo efficient electron bifurcation under the conditions used.

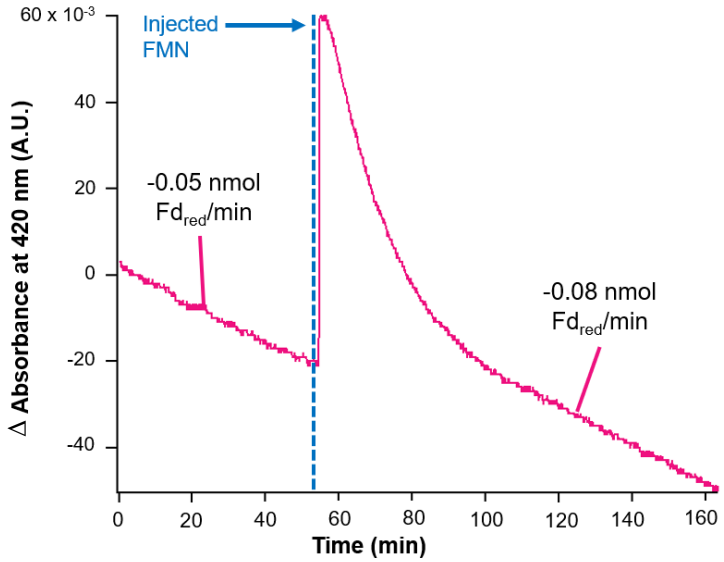


**Figure 3.8** The rate of electron bifurcation before and after addition of an excess of 2 mM FMN was evaluated by measuring the absorbance change at 425 nm, which corresponds to the rate of $Fd_{red}$ produced per minute. The sample contained 200 nM *Amo* hydrogenase, 100 uM *Pfu* Fd, and 1 mM $NAD^+$, in a pH 8 buffer of 100 mM MPA and 50 mM potassium phosphate under 5% $H_2$ headspace.

It is meaningful that the system showed no evidence of electron confurcation in the hydrogen production assays but could easily be driven to perform electron bifurcation under nearly identical conditions. The primary difference between the two sets of reaction conditions is

that the hydrogen production assays are light-driven with QDs, while electron bifurcation is catalyzed by putting the reaction under an $H_2$ atmosphere and contains no nanomaterials. Given this difference, it seems possible that the QDs are interfering with the electron bifurcation mechanism, possibly by binding to the enzyme in a way that prevents the necessary conformational changes from occurring.

### *3.3.4 Photoluminescence Quenching of CdSe Quantum Dots*

To test the binding behavior of the QDs to *Amo* hydrogenase, a photoluminescence quenching assay was performed. As demonstrated in **Figure 3.9**, the intensity of emitted light increases as *Amo* hydrogenase is added to the solution. This provides evidence that the QDs bind to *Amo* hydrogenase but does not directly transfer electrons to the enzyme, instead increasing fluorescence through surface passivation of the nanomaterials. This provides support for the hypothesis that binding of QDs to *Amo* hydrogenase inhibits electron bifurcation.

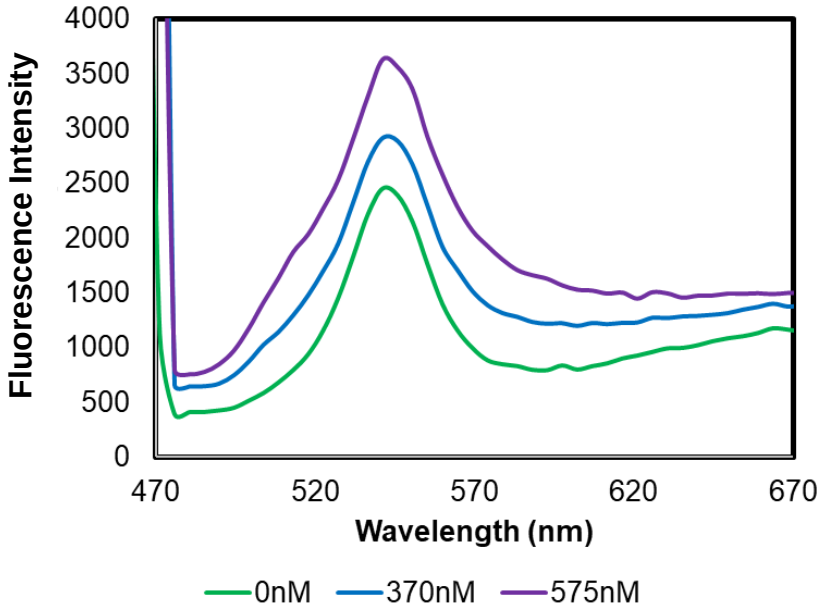


**Figure 3.9** Photoluminescence quenching experiment shows that increasing the concentration of *Amo* hydrogenase causes an increase in fluorescence intensity of QD 3.

## 3.4 References

1. Feng, X.; Schut, G.; Haja, D.; Adams, M.; Huilin, L. Structure and electron transfer pathways of an electron-bifurcating NiFe-hydrogenase. *Sci. Adv.* **2022**, *8*(8).

2. Narehood, S. (2020). Optimization of Electron Bifurcation Photocatalytic System. [Undergraduate honors thesis]. Emory University.

3. NIST Chemistry WebBook. Hydrogen. https://webbook.nist.gov/cgi/cbook.cgi?ID=C1333740&Mask=10

4. Bac*Dive*: doi: 10.1093/nar/gkab961

5. Adams, M.; Mortenson, L.; Chen, J. Hydrogenase. *BBA*. **1980,** *594*(2-3), 105-176.

# Chapter 4: Conclusions and Perspectives

## 4.1 Aim 1: Engineering Effective Photosensitive Nanomaterials

Synthesis and characterization of CdSe QDs and CdSe/CdS DIRs led to the discovery of photosensitizers with the desired optical and electronic properties. TEM imaging revealed uniform shape and size distributions, and ligand exchange with MPA kept the QDs and DIRs from aggregating in solution. The obtained nanomaterials satisfied all criteria put forth: their UV-Visible absorbance spectrum had minimal overlap with that of cofactors in the hydrogenase system, and they had high quantum yields between 30-90%. Although none of the nanomaterials synthesized had a maximum absorbance peak exactly at the excitation wavelength (532 nm), high quantum yields indicated that this was not ultimately a problem. However, the nanomaterials could be further optimized by tuning their optical properties to absorb more light with a wavelength of 532 nm for increased efficiency and to minimize the concentration needed.

Although the photosensitizers we engineered met the criteria we laid out for success, we did not anticipate that they would bind to *Amo* Fd and prevent electron confurcation. From this perspective, the nanomaterials used in our experiments were not optimal for the system. To achieve confurcation, the system requires photosensitizers that electrostatically bind to *Amo* Fd but not to the HydABCSL enzyme. Achieving this balance is difficult, but a first step would be to determine the binding coefficient between the QDs and each of the proteins using a photoluminescence quenching assay and Langmuir isotherm. Subsequently, the surface charge of the photosensitizers could be tuned by varying the attached capping ligands to make them either less negatively charged or positively charged. For instance, using glutathione ligands would reduce the negative surface charge of the photosensitizers and possibly weaken interaction with the hydrogenase enzyme.

## 4.2 Aim 2: Achieving Light Driven Reduction of *Amo* Ferredoxin

We demonstrate successful light-driven electron transfer between the photosensitizers and both *Pfu* and *Amo* Fd through steady state experiments. This encouraging result indicates compatibility between the nanomaterials and bifurcating hydrogenase system. Reduction of *Pfu* Fd appears to be more favored than reduction of *Amo* Fd, either kinetically or thermodynamically. Ultrafast spectroscopic experiments could provide further insight into the

kinetics of electron transfer between the photosensitizers and Fd and give rationale for the observed differences in Fd reduction between the two species.

### 4.3 Aim 3: Identifying Optimal Conditions for $H_2$ Production via Electron Bifurcation

Although minimal amounts of $H_2$ were generated in the hydrogen production assays, the rates were not large enough to indicate that electron confurcation successfully took place. However, the experimental conditions themselves did not appear to be the factor impeding the confurcation reaction. We show that hydrogenase is sufficiently active at 20°C, *Amo* Fd is efficiently reduced by the photosensitizers, Fd successfully transfers electrons to hydrogenase, the FMN concentration is adequate, and that the conditions are suitable for electron bifurcation in the absence of nanomaterials. Collectively, this evidence points towards inhibitive interactions between the nanomaterials and HydABCSL that prevent electron confurcation from taking place under otherwise suitable conditions. Admittedly, this evidence is circumstantial and factors that remain unconsidered, such as a lack of sufficient concentrations of NADH or Fd, could also contribute to the inability of the system to confurcate electrons. However, our hypothesis is further corroborated by a photoluminescence quenching assay that shows binding of QDs to the enzyme without direct electron transfer.

### 4.4 Implications and Future Directions

Our results provide insight into the mechanism of HydABCSL and a scaffold for further efforts to engineer an artificial photosynthetic system that uses electron confurcation. We have discovered that CdSe QDs bind to HydABCSL in a way that blocks electron confurcation from occurring. This provides further evidence that conformational changes are crucial to the electron confurcation mechanism. A future experiment could utilize cryo-EM to characterize where the QDs bind to the hydrogenase enzyme and the conformational state it locks the enzyme into. Combining evidence from this thesis that the QD-bound enzyme cannot facilitate electron confurcation with structural information from cryo-EM would reveal new details about the mechanism and pathway of electron transfer through the enzyme. This thesis also lays the groundwork for eventually optimizing the proposed system for $H_2$ production by using QD capping ligands that avoid interactions with hydrogenase. Such a system would have applications in generating hydrogen solar fuel and could be easily studied further using time-resolved spectroscopic methods to better understand the intermediate states of electron confurcation.